

Anisotropic decay of the energy spectrum in two-dimensional dense granular flows

Kuniyasu Saitoh¹ and Hideyuki Mizuno²¹WPI-Advanced Institute for Materials Research, Tohoku University, 2-1-1 Katahira, Aoba-ku, Sendai 980-8577, Japan²Graduate School of Arts and Sciences, The University of Tokyo, Tokyo 153-8902, Japan

(Received 4 January 2017; revised manuscript received 21 June 2017; published 12 July 2017)

We study anisotropic collective motions of two-dimensional granular particles under simple shear deformations. Employing molecular-dynamics simulations of large system sizes, we find that anisotropic fluidized bands develop in the system yielding under quasistatic deformations, where the spectrum of nonaffine velocities, which is associated with the energy spectrum for turbulent flows, exhibits a quadrupole structure. To explain theoretically the anisotropic spectrum, we derive hydrodynamic modes from a continuum model of dense granular materials, where we find that fluidized bands are caused by long-lived hydrodynamic fluctuations characterized by compressibility.

DOI: [10.1103/PhysRevE.96.012903](https://doi.org/10.1103/PhysRevE.96.012903)

I. INTRODUCTION

Dense granular materials have wide applications in industry, and the study of their flow behavior has long been of practical importance to technology [1]. When granular materials flow by external forces, the injected energy is dissipated through inelastic interactions between constituent particles so that kinetic energy is transferred from macro- to microscopic scales [2–4]. Due to this nonequilibrium nature, microscopic origins of their flow properties have not yet been fully understood, e.g., kinetic theory of inelastic particles succeeds in describing the rheology of granular gases [5], while it fails to explain the rate-independent flow behavior of yielding granular materials [6,7], i.e., the so-called *critical state* in soil mechanics [1]. Therefore, in the past few decades, the microscopic insight into dense granular flows has been widely investigated via experiments and numerical simulations, where turbulent-like collective motions of the particles around mean flow were commonly observed [8–13].

In those previous studies, nonaffine components of particle displacements or velocities, which are the direct measure of particle rearrangements around mean flow, were assumed to be isotropic in space. However, anisotropic collective rearrangements were recently reported in molecular-dynamics (MD) simulations of supercooled liquids [14], and the directional dependence of their spatial correlation functions was found in experiments of sheared suspensions [15–17] and MD simulations of athermal particles under shear [18–20]. Therefore, it is crucial to clarify anisotropic motions of constituent particles behind the anomalous rheology of dense granular materials, which we investigate numerically and explain theoretically in this paper.

We show our numerical simulations in Sec. II and explain our numerical results by a continuum theory in Sec. III. Then, we conclude and discuss our results in Sec. IV.

II. NUMERICAL SIMULATIONS

We study two-dimensional granular flows by MD simulations of frictional particles [21]. To avoid crystallization, we use 50:50 binary mixtures of N particles, where different kinds of particles have the same mass, m , and different diameters (their ratio is 1.4). The force between the particles in contact is

divided into the normal and tangential directions: The normal force, f_n , is modeled by a linear spring-dashpot, where the spring constant and viscosity coefficient are given by k_n and η_n , respectively. The tangential force, f_t , is also described by the linear spring-dashpot with the same spring constant and viscosity coefficient, i.e., $k_t = k_n$ and $\eta_t = \eta_n$, respectively, while it switches to dynamical friction if it exceeds a threshold, i.e., if $|f_t| > \mu_m |f_n|$ with a friction coefficient, $\mu_m = 0.5$ [22]. In our simulations, the normal restitution coefficient is estimated as $e_n = \exp(-\pi/\sqrt{2k_n\eta_n^{-2} - 1}) \simeq 0.7$ [21] and a unit of time is introduced as $t_m \equiv \eta_n/k_n = \eta_t/k_t$.

We randomly distribute the N particles in an $L \times L$ square periodic box such that the area fraction of the particles is given by ϕ_0 . Then, we apply simple shear deformations to the system by the Lees-Edwards boundary condition [23]. In each time step, every particle position, $\mathbf{r}_i = (x_i, y_i)$, is replaced with $(x_i + \Delta\gamma y_i, y_i)$ ($i = 1, \dots, N$) and equations of translational and rotational motions are numerically integrated with a small time increment, $\Delta t = 4 \times 10^{-3} t_m$ [21]. Here, $\Delta\gamma$ is a small strain increment so that the shear rate is defined as $\dot{\gamma} \equiv \Delta\gamma/\Delta t$. In the following analyses, we scale every mass, time, and length by m , t_m , and mean particle diameter, d_m , respectively.

In our MD simulations, the mean velocity field is determined by the affine deformation as $\dot{\gamma} y \mathbf{e}_x$, where y and \mathbf{e}_x are the y coordinate and unit vector along the x axis, respectively. On the other hand, complicated rearrangements of the particles around the mean velocity field can be analyzed by *nonaffine velocities*, $\delta \mathbf{u}_i \equiv \mathbf{u}_i - \dot{\gamma} y_i \mathbf{e}_x$, where \mathbf{u}_i is the velocity of the i th particle. Recently, anomalous statistics of nonaffine velocities have been extensively studied, e.g., their probability distributions showed tails much wider than those of Gaussian distributions [10] and their spatial correlations revealed that the collective behavior became significant in quasistatic flows [11]. In addition, the spectrum of nonaffine velocities [9], which was introduced by analogy with the *energy spectrum* for turbulence, exhibited power-law decay on a mesoscopic scale so that turbulent-like structures of nonaffine velocities were inherent in two-dimensional dense granular flows [3]. In those analyses, however, spatial distributions of nonaffine velocities were assumed to be isotropic, which is not the case if the system size is large enough.

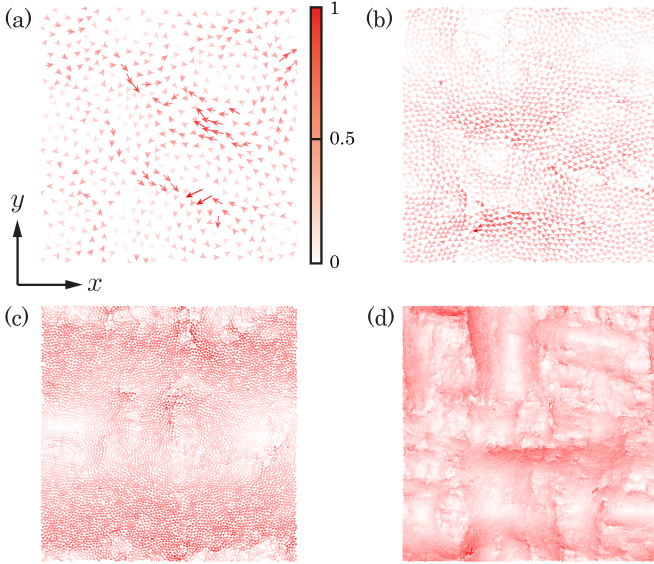


FIG. 1. The system size dependence of nonaffine velocities (the arrows), where the number of particles is given by (a) $N = 512$, (b) $N = 2048$, (c) $N = 8192$, and (d) $N = 32768$. The gray scale represents the magnitude of nonaffine velocities scaled by the maximum, i.e., $|\delta\mathbf{u}_i|/|\delta\mathbf{u}_m|$ ($i = 1, \dots, N$). The control parameters, $\phi_0 = 0.84$ and $\dot{\gamma}t_m = 2.5 \times 10^{-5}$, are used in MD simulations.

Figure 1 displays our numerical results of the nonaffine velocities (snapshots in steady states [24]), where we change the number of particles from (a) $N = 512$ to (d) $N = 32768$. In this figure, no preferred direction of the nonaffine velocities can be seen if the system size is too small [Figs. 1(a) and 1(b)], while they tend to align in the x or y direction as their collective motions form anisotropic *fluidized bands* [14] in large system sizes [Figs. 1(c) and 1(d)]. As shown in Appendix A, the nonaffine velocities are dynamically changing during steady state so that the anisotropic bandlike structures are not permanent shear-banding. In addition, we have confirmed that anisotropic collective motions were observed only if the area fraction exceeded a critical value, $\phi_0 > \phi_c \simeq 0.8$, and the shear rate was extremely small, $\dot{\gamma}t_m \ll 1$, such that rate-independent yield stress can be observed [3].

To quantify the anisotropic collective behavior of nonaffine velocities, we introduce their spectrum as a function of two-dimensional wave number vector, $\mathbf{k} = (k_x, k_y)$, i.e.,

$$E(\mathbf{k}) = \frac{mn_0}{2} \langle |\delta\hat{\mathbf{u}}(\mathbf{k})|^2 \rangle, \quad (1)$$

where $n_0 \equiv N/L^2$ is the number density and $\delta\hat{\mathbf{u}}(\mathbf{k}) = n_0^{-1} \sum_{i=1}^N \delta\mathbf{u}_i e^{-I\mathbf{k}\cdot\mathbf{r}_i}$, where the imaginary unit I is the Fourier transform of nonaffine velocities. In Eq. (1), the angular brackets represent time average during steady state, where the applied strain is in the range between $1 < \gamma < 2$. In addition, the spectrum is defined as the Fourier transform of the (equal-time) spatial correlation function of the nonaffine velocity field [25] and thus is neither dependent on time during steady state nor stretched along the sheared direction [26], as is the case with a static structure factor under simple shear deformations [27,28]. The spectrum, Eq. (1), was first introduced in the numerical study of granular flows under

constant pressure [9], where it was averaged over all the directions of \mathbf{k} , i.e., $E(k)$ with the wave number $k \equiv |\mathbf{k}|$ by assuming isotropic distributions of nonaffine velocities. Because the integral $\int E(\mathbf{k})d\mathbf{k}$ is associated with *granular temperature* [5], the spectrum, Eq. (1), quantifies the density of fluctuation energy in different scales and directions.

Figure 2 shows logarithmic plots of the spectra in units of mass, time, and length, i.e., m , t_m , and d_m , respectively, where the system size, $N = 131072$, is large enough to observe anisotropic collective motions. In this figure, we increase the area fraction ϕ_0 and shear rate $\dot{\gamma}t_m$ in MD simulations as indicated by the arrows, where the spectra exhibit *quadrupole structures* if $\phi_0 > \phi_c$ and $\dot{\gamma}t_m \ll 1$, which is a result of fluidized bands developed along the x and y axes [Fig. 1(d)]. Such a quadrupole structure in Fourier space was first unveiled by the spectrum of nonaffine displacements in supercooled liquids, where the shear rate was large enough for the particles to overcome random thermal forces, and the shear-induced anisotropic cage breaking occurred [14]. In granular materials, however, the particles are not affected by thermal fluctuations and immediately show anisotropic rearrangements around mean flows, where their collective motions enhanced in yielding and the quasistatic regime, i.e., $\phi_0 > \phi_c$ and $\dot{\gamma}t_m \ll 1$ [3], induce the large-scale fluidized bands. Moreover, similar quadrupole patterns were also observed in spatial correlations of plastic strains in sheared suspensions [16] as well as athermal particles under shear [19,20]. We also confirm that the static structure factor is quite insensitive to the area fraction and is more isotropic if the shear rate is small (data are not shown) [17,27,28]. Therefore, we suppose that the anisotropy of nonaffine velocities, which we explain theoretically below, is not caused by particle configurations under shear.

III. THEORY

To explain the anisotropic decay of spectra, we adopt a continuum model of two-dimensional dense granular materials [29]. In this model, the area fraction, $\phi(\mathbf{r}, t)$, velocity field, $\mathbf{u}(\mathbf{r}, t) = (u_x, u_y)$, and granular temperature, $\theta(\mathbf{r}, t)$, are defined as hydrodynamic fields, where \mathbf{r} and t represent position and time, respectively. Then, their time development is described by hydrodynamic equations,

$$D_t \phi = -\phi \nabla_\alpha u_\alpha, \quad (2)$$

$$\phi D_t u_\alpha = \nabla_\beta \sigma_{\alpha\beta}, \quad (3)$$

$$\phi D_t \theta = \sigma_{\alpha\beta} \nabla_\alpha u_\beta - \nabla_\alpha q_\alpha - \chi, \quad (4)$$

where the Einstein convention is used for the subscripts α and β ($=x, y$). On the left-hand sides, $D_t \equiv \partial/\partial t + u_\alpha \nabla_\alpha$ represents the material derivative. On the right-hand sides of Eqs. (3) and (4), the stress tensor and heat flux are given by the usual forms, i.e., $\sigma_{\alpha\beta} = \eta(\nabla_\alpha u_\beta + \nabla_\beta u_\alpha) + \delta_{\alpha\beta}\{(\xi - \eta)\nabla_\nu u_\nu - p\}$ and $q_\alpha = -\kappa \nabla_\alpha \theta$, respectively ($\nu = x, y$), where p , η , ξ , and κ are the pressure, shear viscosity, bulk viscosity, and thermal conductivity, respectively. On the right-hand side of Eq. (4), the last term, $\chi \equiv \phi\theta\zeta$, represents *energy dissipation* in the bulk, which is caused by inelastic interactions between the

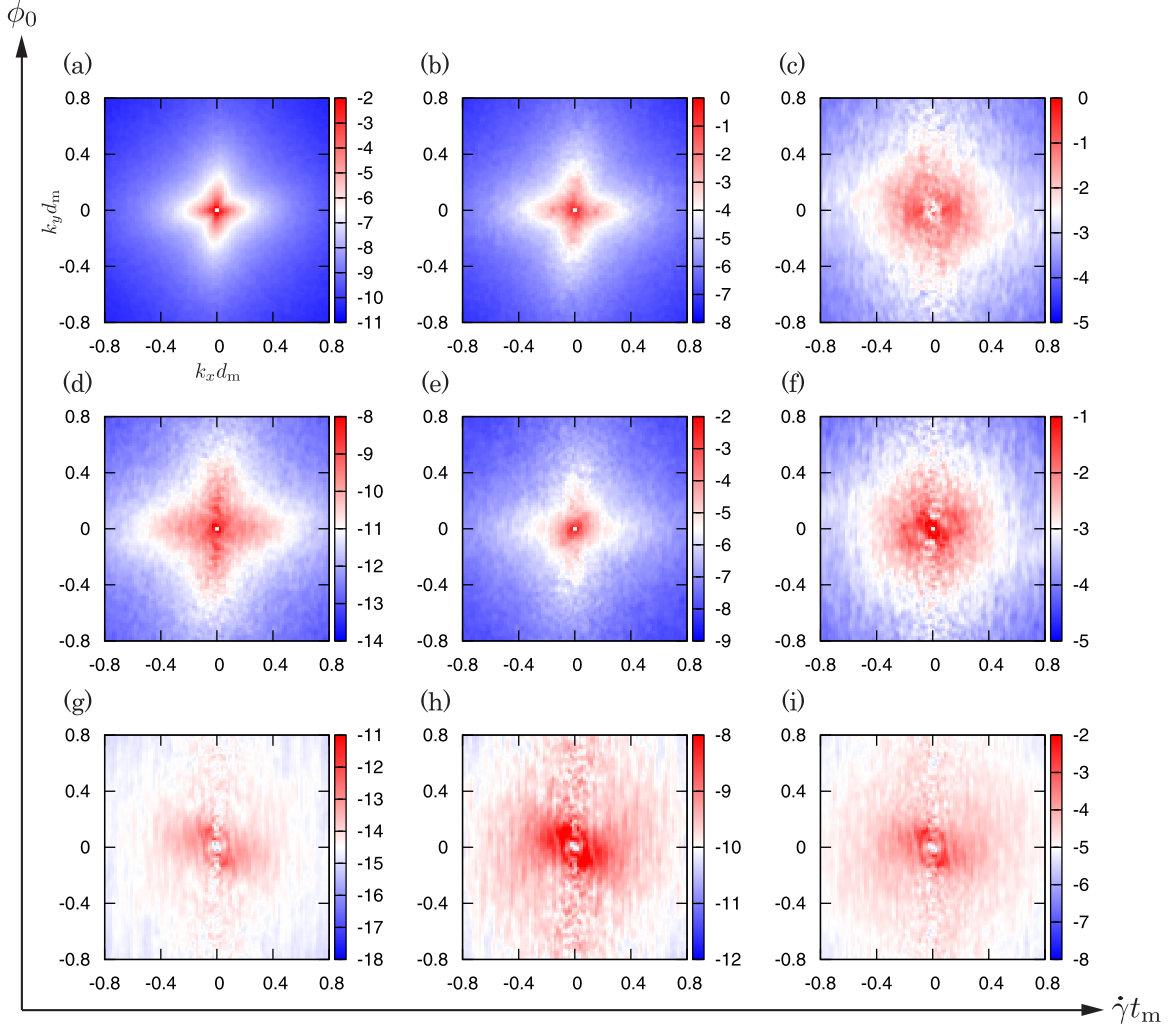


FIG. 2. Three-dimensional plots of logarithmic spectra, $\log E(\mathbf{k})$, where each component of the wave number vector is scaled by the mean particle diameter [as shown only in (a)]. The number of particles is given by $N = 131\,072$, and the control parameters, i.e., ϕ_0 and $\dot{\gamma}t_m$, increase as indicated by the arrows, where $\phi_0 =$ (a)–(c) 0.84, (d)–(f) 0.80, and (g)–(i) 0.70, and $\dot{\gamma}t_m =$ (a),(d),(g) 2.5×10^{-5} , (b),(e),(h) 2.5×10^{-4} , and (c),(f),(i) 2.5×10^{-3} are used in MD simulations.

particles in contact, where ζ is introduced as a dissipation rate [29].

In dense granular materials, not only individual motions of the particles (i.e., a gaslike *kinetic contribution*), but also contact forces between them (i.e., a solidlike *contact contribution*) contribute to the stress. Therefore, in this model, the pressure consists of kinetic and contact parts as $p = p_{\text{kin}} + p_{\text{con}}$ [29]. The kinetic part is derived from kinetic theory of granular gases as $p_{\text{kin}} = [1 + (1 + e_n)G(\phi)]\phi\theta$ [5], where we use the global fitting model for the pair correlation function at contact, $G(\phi)$ [30]. On the other hand, the contact part is given by $p_{\text{con}} = a_0 \log\{(\phi_\infty - \phi_c)/(\phi_\infty - \phi)\}$ with a reference value a_0 , where ϕ_∞ is introduced as the area fraction corresponding to the closest packing [29]. The contact part, p_{con} , is zero if the area fraction equals the critical value ($\phi = \phi_c$), while it diverges if the area fraction approaches the maximum ($\phi \rightarrow \phi_\infty$). Thus, it should be noted that the model can be used in the range between $\phi_c < \phi < \phi_\infty$. The input parameters, $a_0 = 3.25 \times 10^{-2}k_n$ and $\phi_\infty = 0.9$, have been adjusted to our numerical results of pressure [3], and

the normal restitution coefficient and critical area fraction are estimated from our MD simulations as $e_n = 0.7$ and $\phi_c = 0.8$, respectively [3]. In addition to the pressure, the transport coefficients (η, ξ, κ) and energy dissipation (χ) are also divided into the kinetic and contact parts, e.g., $\eta = \eta_{\text{kin}} + \eta_{\text{con}}$ [29].

Next, we divide the hydrodynamic fields into homogeneous fields and fluctuations as $\phi(\mathbf{r}, t) = \phi_0 + \delta\phi(\mathbf{r}, t)$, $\theta(\mathbf{r}, t) = \theta_0 + \delta\theta(\mathbf{r}, t)$, and $\mathbf{u}(\mathbf{r}, t) = \epsilon y \mathbf{e}_x + \delta\mathbf{u}(\mathbf{r}, t)$, where $\epsilon \equiv \dot{\gamma}t_m$ is the scaled shear rate, and the homogeneous granular temperature, θ_0 , is determined by substituting the homogeneous fields into the equation of granular temperature, Eq. (4). Note that $\delta\mathbf{u}(\mathbf{r}, t) = (\delta u_x(\mathbf{r}, t), \delta u_y(\mathbf{r}, t))$ is equivalent to the nonaffine velocity field. Then, expanding the pressure, transport coefficients, and energy dissipation into the Taylor series in $\delta\phi(\mathbf{r}, t)$ and $\delta\theta(\mathbf{r}, t)$, we linearize the hydrodynamic equations (2)–(4) around the homogeneous fields (see Appendix B 1). Applying the Fourier transform to the fluctuations as $\hat{\phi}_{\mathbf{k}}(t) = \int \phi(\mathbf{r}, t) e^{-i\mathbf{k}\cdot\mathbf{r}} d\mathbf{r}$ with $\phi(\mathbf{r}, t) \equiv (\delta\phi(\mathbf{r}, t), \delta\theta(\mathbf{r}, t), I^{-1}\delta\mathbf{u}(\mathbf{r}, t))^T$, we find that the *hydrodynamic mode*, $\hat{\phi}_{\mathbf{k}}(t) \equiv (\delta\hat{\phi}_{\mathbf{k}}(t), \delta\hat{\theta}_{\mathbf{k}}(t), \delta\hat{\mathbf{u}}_{\mathbf{k}}(t))^T$, satisfies the linearized

hydrodynamics [31],

$$\frac{\partial}{\partial t} \hat{\phi}_{\mathbf{k}}(t) = \left(\mathcal{L} + \epsilon k_x \frac{\partial}{\partial k_y} \right) \hat{\phi}_{\mathbf{k}}(t), \quad (5)$$

where \mathcal{L} is the 4×4 hydrodynamic matrix, and the anisotropic operator, $\epsilon k_x \partial / \partial k_y$, originates from the convection term [26]. Because the linear operator on the right-hand side, i.e., $\mathcal{L} + \epsilon k_x \partial / \partial k_y$, is time-independent, we rewrite the hydrodynamic mode as $\hat{\phi}_{\mathbf{k}}(t) \propto \hat{\psi}_{\mathbf{k}}^{(l)} e^{\lambda^{(l)} t}$ so that Eq. (5) is reduced to an eigenvalue problem, $(\mathcal{L} + \epsilon k_x \partial / \partial k_y) \hat{\psi}_{\mathbf{k}}^{(l)} = \lambda^{(l)} \hat{\psi}_{\mathbf{k}}^{(l)}$, where $\lambda^{(l)}$ and $\hat{\psi}_{\mathbf{k}}^{(l)} \equiv (\delta \hat{\phi}_{\mathbf{k}}^{(l)}, \delta \hat{\theta}_{\mathbf{k}}^{(l)}, \delta \hat{\mathbf{u}}_{\mathbf{k}}^{(l)})^T$ are the l th eigenvalue and eigenvector, respectively ($l = 1, \dots, 4$).

In Appendix B 2, we solve the eigenvalue problem by *perturbation theory*, where the scaled shear rate, ϵ , is used as the expansion parameter because the anisotropic decay of the spectrum, Eq. (1), is pronounced if $\epsilon \ll 1$ (Fig. 2). Then, we find that each eigenvector is given by

$$\hat{\psi}_{\mathbf{k}}^{(1)} \simeq \begin{pmatrix} \{p_\theta / J\} + \epsilon \{\sqrt{2} \phi_0^2 / J\} f_3^{(1)} \\ -\{p_\phi / J\} + \epsilon \{\sqrt{2} p_0 / J\} f_3^{(1)} \\ \epsilon \{\hat{k}_y f_2^{(1)} - \sqrt{2} \hat{k}_x g_3^{(1)}\} \\ -\epsilon \{\hat{k}_x f_2^{(1)} + \sqrt{2} \hat{k}_y g_3^{(1)}\} \end{pmatrix}, \quad (6)$$

$$\hat{\psi}_{\mathbf{k}}^{(2)} \simeq \begin{pmatrix} \epsilon \{[p_\theta / J] f_1^{(2)} + \{\sqrt{2} \phi_0^2 / J\} f_3^{(2)}\} \\ \epsilon [-\{p_\phi / J\} f_1^{(2)} + \{\sqrt{2} p_0 / J\} f_3^{(2)}] \\ \hat{k}_y - \epsilon \sqrt{2} \hat{k}_x g_3^{(2)} \\ -\hat{k}_x - \epsilon \sqrt{2} \hat{k}_y g_3^{(2)} \end{pmatrix}, \quad (7)$$

$$\hat{\psi}_{\mathbf{k}}^{(3)} \simeq \begin{pmatrix} \frac{\phi_0^2}{\sqrt{2} J} + \epsilon \frac{\phi_0^2 f_4^{(3)} + \sqrt{2} p_\theta f_1^{(3)}}{\sqrt{2} J} + I \epsilon \frac{\phi_0^2 g_4^{(3)} + \sqrt{2} p_\theta g_1^{(3)}}{\sqrt{2} J} \\ \frac{p_0}{\sqrt{2} J} + \epsilon \frac{p_0 f_4^{(3)} - \sqrt{2} p_\phi f_1^{(3)}}{\sqrt{2} J} + I \epsilon \frac{p_0 g_4^{(3)} - \sqrt{2} p_\phi g_1^{(3)}}{\sqrt{2} J} \\ \frac{I \hat{k}_x}{\sqrt{2}} + \epsilon \frac{\hat{k}_x g_4^{(3)} + \sqrt{2} \hat{k}_y f_2^{(3)}}{\sqrt{2}} + I \epsilon \frac{\sqrt{2} \hat{k}_y g_2^{(3)} - \hat{k}_x f_4^{(3)}}{\sqrt{2}} \\ \frac{I \hat{k}_y}{\sqrt{2}} + \epsilon \frac{\hat{k}_y g_4^{(3)} - \sqrt{2} \hat{k}_x f_2^{(3)}}{\sqrt{2}} - I \epsilon \frac{\sqrt{2} \hat{k}_x g_2^{(3)} + \hat{k}_y f_4^{(3)}}{\sqrt{2}} \end{pmatrix}, \quad (8)$$

and $\hat{\psi}_{\mathbf{k}}^{(4)} \simeq \hat{\psi}_{\mathbf{k}}^{(3)*}$, in the first-order approximation of ϵ , where $\hat{k}_\alpha \equiv k_\alpha / k$ represents the α -component of the normalized wave number vector ($\alpha = x, y$), and the asterisk, $*$, indicates the complex conjugate. Here, the real functions of wave numbers, e.g., $f_1^{(2)}$, are listed in Table I.

A theoretical expression of the spectrum, Eq. (1), can be given by the superposition of l th eigenvectors, i.e., $E(\mathbf{k}) = |\sum_{l=1}^4 c_l \delta \hat{\mathbf{u}}_{\mathbf{k}}^{(l)}|^2$ with coefficients c_l . However, we examine the spectrum of each eigenvector, i.e., $E_l(\mathbf{k}) = |\delta \hat{\mathbf{u}}_{\mathbf{k}}^{(l)}|^2$, to understand the effect of each mode on the anisotropic collective behavior [Fig. 2(a)]. Figure 3 compares our numerical result of the spectrum, $E(\mathbf{k})$, with the theoretical expressions, $E_l(\mathbf{k})$, where the first mode ($l = 1$) explains well the quadrupole structure [Figs. 3(a) and 3(b)], while the others are almost constant, i.e., $E_2(\mathbf{k}) \simeq 1$ and $E_3(\mathbf{k}) = E_4(\mathbf{k}) \simeq 1/2$ [Figs. 3(c) and 3(d)]. Note that the eigenvalue for the first mode is given by $\lambda^{(1)} \simeq -(\phi_0 \kappa_0 k^2 / J^2) (\partial p / \partial \phi)$ (see the symbols in Table I) so that the relaxation time of the first mode, $\tau_1 \equiv -1 / \lambda^{(1)}$,

TABLE I. Real functions of wave numbers, k_x , k_y , and $k \equiv \sqrt{k_x^2 + k_y^2}$, for the approximate eigenvectors, Eqs. (6)–(8), where $J \equiv \sqrt{p_0 p_\theta + \phi_0^2 p_\phi}$ and $A \equiv (\eta_0 + \xi_0 + \kappa_0 p_0 p_\theta / J^2) / 2 \phi_0$. The subscript 0 means the value for a homogeneous state, while the subscripts ϕ and θ represent the derivatives with respect to the area fraction and granular temperature, respectively.

$f_1^{(2)}$	$= -\frac{2\phi_0^2 \eta_0 J}{\eta_0 J^2 - \phi_0^2 \kappa_0 p_\phi} \frac{k_y^2 - k_x^2}{k^3}$
$f_1^{(3)}$	$= \frac{2\sqrt{2} \phi_0^2 \eta_0 J^4}{\phi_0^2 (\phi_0 \kappa_0 p_\phi - A J^2)^2 k^2 + J^6} \frac{k_x k_y}{k^2}$
$g_1^{(3)}$	$= \frac{2\sqrt{2} \phi_0^3 \eta_0 J (\phi_0 \kappa_0 p_\phi - A J^2)}{\phi_0^2 (\phi_0 \kappa_0 p_\phi - A J^2)^2 k^2 + J^6} \frac{k_x k_y}{k}$
$f_2^{(1)}$	$= \frac{J (p_\theta \eta_\phi - p_\phi \eta_\theta)}{\eta_0 J^2 - \phi_0^2 \kappa_0 p_\phi} \frac{k_y^2 - k_x^2}{k^3}$
$f_2^{(3)}$	$= \frac{(\eta_0 - \phi_0 A) (\phi_0^2 \eta_\phi + p_0 \eta_\theta) (k_y^2 - k_x^2) - J^2}{\sqrt{2} J [(\eta_0 - \phi_0 A)^2 k^2 + J^2] k}$
$g_2^{(3)}$	$= \frac{(\phi_0^2 \eta_\phi + p_0 \eta_\theta) (k_x^2 - k_y^2) - \phi_0 (\eta_0 - \phi_0 A) k^2}{\sqrt{2} \phi_0 [(\eta_0 - \phi_0 A)^2 k^2 + J^2] k^2}$
$f_3^{(1)}$	$= \frac{\sqrt{2} J^4 (p_\theta \eta_\phi - p_\phi \eta_\theta)}{\phi_0^2 (\phi_0 \kappa_0 p_\phi - A J^2)^2 k^2 + J^6} \frac{k_x k_y}{k^2}$
$g_3^{(1)}$	$= \frac{\sqrt{2} \phi_0 J (p_\theta \eta_\phi - p_\phi \eta_\theta) (\phi_0 \kappa_0 p_\phi - A J^2)}{\phi_0^2 (\phi_0 \kappa_0 p_\phi - A J^2)^2 k^2 + J^6} \frac{k_x k_y}{k}$
$f_3^{(2)}$	$= \frac{\sqrt{2} \{ \phi_0 J^2 k_x^2 - p_\theta \eta_0 (\eta_0 - \phi_0 A) (k_y^2 - k_x^2) k^2 \}}{[(\eta_0 - \phi_0 A)^2 k^2 + J^2] J k^3}$
$g_3^{(2)}$	$= \frac{\sqrt{2} \{ p_\theta \eta_0 (k_x^2 - k_y^2) + \phi_0 (\eta_0 - \phi_0 A) k_x^2 \}}{[(\eta_0 - \phi_0 A)^2 k^2 + J^2] k^2}$
$f_4^{(3)}$	$= \frac{\phi_0^2 \eta_\phi + p_0 \eta_\theta - 2 p_0 \eta_0}{2 J^2} \frac{k_x k_y}{k^2}$
$g_4^{(3)}$	$= -\frac{\phi_0}{4 J} \frac{k_x k_y}{k^3}$

is proportional to the compressibility, i.e., $\tau_1 \propto k^{-2} \beta_s$ with $\beta_s \equiv (\partial p / \partial \phi)^{-1}$. We also confirm that the relaxation time of the first mode is the longest one (Appendix C 2). Therefore, we conclude that anisotropic fluidized bands are generated by the long-lived hydrodynamic fluctuation characterized by the compressibility. In addition, the first mode is immediately suppressed if the system size is too small because the relaxation time, $\tau_1 \propto k^{-2} \beta_s$, becomes shorter with the increase of the wave number, k [32].

IV. SUMMARY

In this study, we have investigated the anisotropic collective behavior of nonaffine velocities in two-dimensional dense granular flows. From MD simulations with large system sizes, we found that fluidized bands developed along the x and y directions [Fig. 1(d)] if the area fraction exceeded a critical value, $\phi_0 > \phi_c$, and the shear rate was extremely small, $\dot{\gamma} t_m \ll 1$, i.e., when the system was yielding under quasistatic deformations. Then, the spectrum, Eq. (1), exhibited quadrupole structures (Fig. 2), representing the strong anisotropy in spatial correlations of nonaffine velocities like the fluidized bands [14]. We found that the hydrodynamic mode derived from a continuum model well explained the quadrupole structure [Figs. 3(a) and 3(b)], implying that fluidized bands were caused by the hydrodynamic fluctuation with the relaxation time proportional to the compressibility. However, there is still room for improvement on the theoretical expression of the spectrum, which might be achieved by constructing the general solution for the hydrodynamic modes, replacing the radial distribution function in the continuum model, and including higher-order terms in the perturbation theory. In the future,

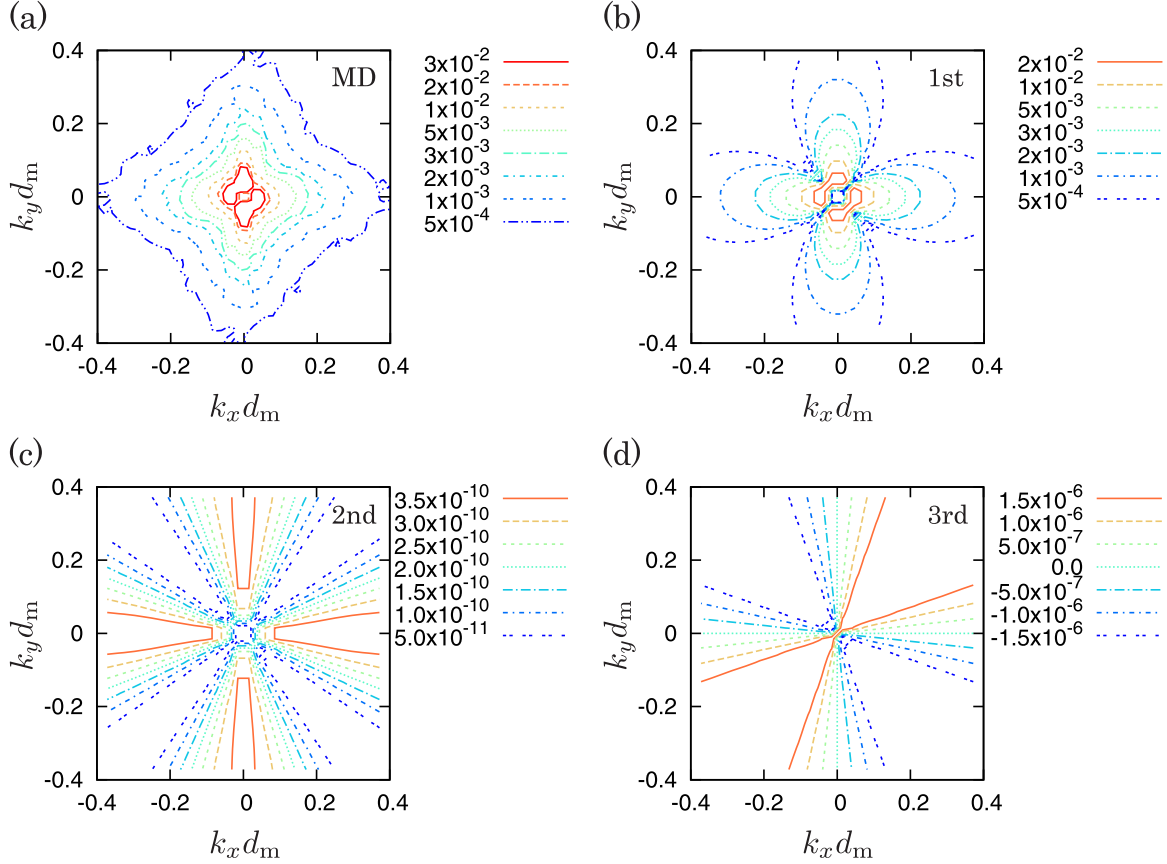


FIG. 3. (a) A contour plot of the spectrum, $E(\mathbf{k})$, obtained from MD simulation. (b)–(d) Contour plots of the spectra of each eigenvector, $E_i(\mathbf{k})$, where (b) $E_1(\mathbf{k})$, (c) $E_2(\mathbf{k}) - 1$, and (d) $E_3(\mathbf{k}) - 1/2$ are plotted. In both the MD simulation and theoretical expressions, the control parameters are as in Fig. 2(a), i.e., $\phi_0 = 0.84$ and $\epsilon \equiv \dot{\gamma} t_m = 2.5 \times 10^{-5}$.

it will be important to extend our analyses of anisotropy to spatiotemporal structures of nonaffine velocities, where the effects on viscoelastic responses [33] and slip avalanches [34] in yielding granular materials should be clarified. Needless to say, the analyses in three dimensions are also crucial to industrial applications of granular materials.

ACKNOWLEDGMENTS

We thank A. Ikeda, H. Hayakawa, M. Otsuki, and T. Kawasaki for fruitful discussions. This work was financially supported by the World Premier International Research Center Initiative (WPI), Ministry of Education, Culture, Sports, Science, and Technology, Japan (MEXT), and Kawai Foundation for Sound Technology & Music. This work was also supported by a Grant-in-Aid for Scientific Research B (No. 16H04025), a Grant-in-Aid for Young Scientists B (No. 17K14369), and a Grant-in-Aid for Research Activity Start-up (No. 16H06628) from the Japan Society for the Promotion of Science (JSPS). A part of the numerical computation has been carried out at the Yukawa Institute Computer Facility, Kyoto, Japan.

APPENDIX A: TIME DEVELOPMENT OF FLUIDIZED BANDS

In this appendix, we show the time development of anisotropic collective motions of granular particles under

simple shear deformations. Figure 4 displays snapshots of nonaffine velocities, $\delta \mathbf{u}_i \equiv \mathbf{u}_i - \dot{\gamma} y_i \mathbf{e}_x$ ($i = 1, \dots, N$), where the shear strain increases from (a) $\gamma = 1.2$ to (d) $\gamma = 1.8$. As can be seen, anisotropic fluidized bands dynamically change during steady state ($1 < \gamma < 2$) such that nonaffine velocities are spatiotemporally fluctuating around the linear velocity profile, $\dot{\gamma} y \mathbf{e}_x$ (though the granular temperature stays constant). On the other hand, the (global) velocity profile remains linear during steady state (Fig. 5) so that the magnitude of nonaffine velocities is much smaller than the (total) velocities. Therefore, it should be noted that anisotropic fluidized bands are not permanent and do not disturb the linear velocity profile, implying that it is not caused by *hydrodynamic instabilities* (or *unstable modes* with positive eigenvalues, $\lambda^{(l)} > 0$) [35–37].

APPENDIX B: HYDRODYNAMIC MODES

In this appendix, we derive theoretical expressions of hydrodynamic modes from the hydrodynamic equations (2)–(4). We introduce *linearized hydrodynamics* in Appendix B 1 and explain our *perturbation theory* in Appendix B 2.

1. Linearized hydrodynamics

The hydrodynamic equations (2)–(4) have a homogeneous solution, i.e., $\phi(\mathbf{r}, t) = \phi_0$, $\theta(\mathbf{r}, t) = \theta_0$, and $\mathbf{u}(\mathbf{r}, t) = \epsilon y \mathbf{e}_x$ with the scaled shear rate, $\epsilon \equiv \dot{\gamma} t_m$. Substituting the homogeneous

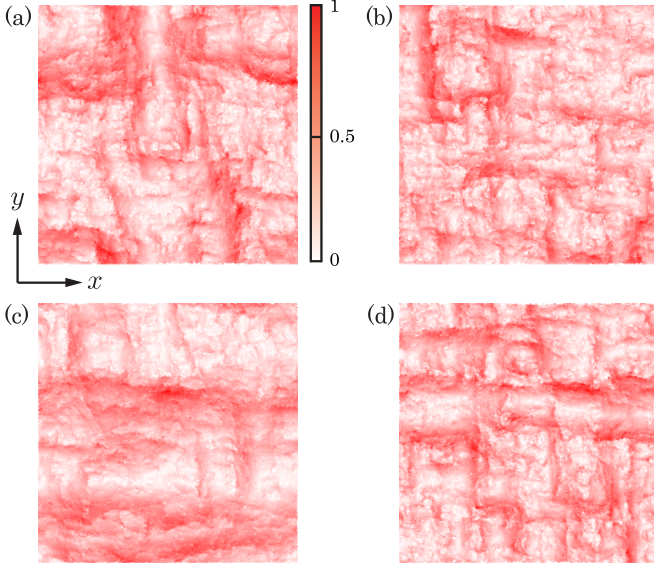


FIG. 4. Time development of nonaffine velocities (arrows), where the applied shear strain is given by (a) $\gamma = 1.2$, (b) $\gamma = 1.4$, (c) $\gamma = 1.6$, and (d) $\gamma = 1.8$. The gray scale represents the magnitude of nonaffine velocities (as in Fig. 1), where $N = 32\,768$, $\phi_0 = 0.84$, and $\dot{\gamma}t_m = 2.5 \times 10^{-5}$ are used in MD simulations.

solution to the equation of granular temperature, we find the balance between the external supply of energy by simple shear deformations and dissipation of kinetic energy due to inelastic interactions as $\epsilon^2 \eta = \chi$. Here, we scale the energy dissipation,

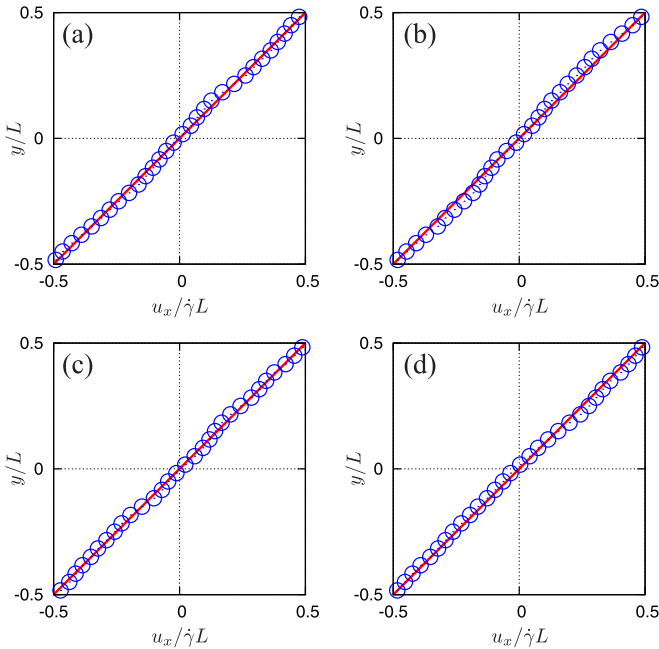


FIG. 5. Time development of the (total) velocity field along the sheared direction, $u_x(y)$ (the blue open circles), where the red solid lines represent the linear velocity profile, $\dot{\gamma}y$. The number of particles, N , the area fraction, ϕ_0 , the scaled shear rate, $\dot{\gamma}t_m$, and the shear strain, γ , in (a)–(d) are as in Fig. 4.

or *inelasticity*, as $\chi \sim \epsilon^2$ so that the mean granular temperature is finite in a steady state.

If we introduce small fluctuations around the homogeneous solution as

$$\phi(\mathbf{r}, t) = \phi_0 + \delta\phi(\mathbf{r}, t), \quad (\text{B1})$$

$$\theta(\mathbf{r}, t) = \theta_0 + \delta\theta(\mathbf{r}, t), \quad (\text{B2})$$

$$\mathbf{u}(\mathbf{r}, t) = \epsilon y \mathbf{e}_x + \delta\mathbf{u}(\mathbf{r}, t), \quad (\text{B3})$$

the pressure, transport coefficients (i.e., bulk viscosity, shear viscosity, and thermal conductivity), and energy dissipation, which are the functions of ϕ and θ , are expanded into the series of small fluctuations as

$$p \simeq p_0 + p_\phi \delta\phi + p_\theta \delta\theta + \dots, \quad (\text{B4})$$

$$\xi \simeq \xi_0 + \xi_\phi \delta\phi + \xi_\theta \delta\theta + \dots, \quad (\text{B5})$$

$$\eta \simeq \eta_0 + \eta_\phi \delta\phi + \eta_\theta \delta\theta + \dots, \quad (\text{B6})$$

$$\kappa \simeq \kappa_0 + \kappa_\phi \delta\phi + \kappa_\theta \delta\theta + \dots, \quad (\text{B7})$$

$$\chi \simeq \chi_0 + \chi_\phi \delta\phi + \chi_\theta \delta\theta + \dots, \quad (\text{B8})$$

respectively, where p_0 , ξ_0 , η_0 , κ_0 , and χ_0 are the values for the homogeneous state (i.e., $\phi = \phi_0$ and $\theta = \theta_0$) and we introduced the derivatives as $p_\alpha \equiv \partial p / \partial \alpha$, $\xi_\alpha \equiv \partial \xi / \partial \alpha$, $\eta_\alpha \equiv \partial \eta / \partial \alpha$, $\kappa_\alpha \equiv \partial \kappa / \partial \alpha$, and $\chi_\alpha \equiv \partial \chi / \partial \alpha$ ($\alpha = \phi, \theta$). Then, introducing coefficients associated with the energy balance as

$$\omega_\alpha \equiv \epsilon^2 \eta_\alpha - \chi_\alpha \quad (\text{B9})$$

($\alpha = 0, \phi, \theta$), we linearize the hydrodynamic equations as

$$\frac{\partial \delta\phi}{\partial t} + \epsilon y \nabla_x \delta\phi \simeq -\phi_0 \nabla_i \delta u_i, \quad (\text{B10})$$

$$\begin{aligned} \frac{\partial \delta u_x}{\partial t} + \epsilon y \nabla_x \delta u_x \\ \simeq (\epsilon \bar{\eta}_\phi \nabla_y - \bar{p}_\phi \nabla_x) \delta\phi + (\epsilon \bar{\eta}_\theta \nabla_y - \bar{p}_\theta \nabla_x) \delta\theta \\ + (\bar{\eta}_0 \nabla^2 + \bar{\xi}_0 \nabla_x^2) \delta u_x + (\bar{\xi}_0 \nabla_x \nabla_y - \epsilon) \delta u_y, \end{aligned} \quad (\text{B11})$$

$$\begin{aligned} \frac{\partial \delta u_y}{\partial t} + \epsilon y \nabla_x \delta u_y \\ \simeq (\epsilon \bar{\eta}_\phi \nabla_x - \bar{p}_\phi \nabla_y) \delta\phi + (\epsilon \bar{\eta}_\theta \nabla_x - \bar{p}_\theta \nabla_y) \delta\theta \\ + (\bar{\eta}_0 \nabla^2 + \bar{\xi}_0 \nabla_y^2) \delta u_y + \bar{\xi}_0 \nabla_x \nabla_y \delta u_x, \end{aligned} \quad (\text{B12})$$

$$\begin{aligned} \frac{\partial \delta\theta}{\partial t} + \epsilon y \nabla_x \delta\theta \\ \simeq \bar{\omega}_\phi \delta\phi + (\bar{\omega}_\theta + \bar{\kappa}_0 \nabla^2) \delta\theta + (2\epsilon \bar{\eta}_0 \nabla_y - \bar{p}_0 \nabla_x) \delta u_x \\ + (2\epsilon \bar{\eta}_0 \nabla_x - \bar{p}_0 \nabla_y) \delta u_y, \end{aligned} \quad (\text{B13})$$

where we introduced scaled quantities as $\bar{p}_\alpha \equiv p_\alpha / \phi_0$, $\bar{\xi}_\alpha \equiv \xi_\alpha / \phi_0$, $\bar{\eta}_\alpha \equiv \eta_\alpha / \phi_0$, $\bar{\kappa}_\alpha \equiv \kappa_\alpha / \phi_0$, and $\bar{\omega}_\alpha \equiv \omega_\alpha / \phi_0$ ($\alpha = 0, \phi, \theta$).

Next, we introduce the Fourier transforms of the fluctuations as

$$\delta\phi(\mathbf{r},t) = \int \delta\hat{\phi}_{\mathbf{k}}(t)e^{I\mathbf{k}\cdot\mathbf{r}}d\mathbf{k}, \quad (\text{B14})$$

$$\delta\theta(\mathbf{r},t) = \int \delta\hat{\theta}_{\mathbf{k}}(t)e^{I\mathbf{k}\cdot\mathbf{r}}d\mathbf{k}, \quad (\text{B15})$$

$$\delta u_x(\mathbf{r},t) = I \int \delta\hat{u}_{x\mathbf{k}}(t)e^{I\mathbf{k}\cdot\mathbf{r}}d\mathbf{k}, \quad (\text{B16})$$

$$\delta u_y(\mathbf{r},t) = I \int \delta\hat{u}_{y\mathbf{k}}(t)e^{I\mathbf{k}\cdot\mathbf{r}}d\mathbf{k}, \quad (\text{B17})$$

with the imaginary unit, I , where $\mathbf{k} = (k_x, k_y)$ is the wave number vector. Here, the Fourier coefficients, i.e., $\delta\hat{\phi}_{\mathbf{k}}(t)$, $\delta\hat{\theta}_{\mathbf{k}}(t)$, $\delta\hat{u}_{x\mathbf{k}}(t)$, and $\delta\hat{u}_{y\mathbf{k}}(t)$, are defined as *hydrodynamic modes* and we find that Eqs. (B10)–(B13) are Fourier-transformed as

$$\frac{\partial}{\partial t}\hat{\phi}_{\mathbf{k}}(t) = \left(\mathcal{L} + \epsilon k_x \frac{\partial}{\partial k_y}\right)\hat{\phi}_{\mathbf{k}}(t), \quad (\text{B18})$$

where the hydrodynamic modes were written in a vector form as $\hat{\phi}_{\mathbf{k}}(t) \equiv (\delta\hat{\phi}_{\mathbf{k}}(t), \delta\hat{\theta}_{\mathbf{k}}(t), \delta\hat{u}_{x\mathbf{k}}(t), \delta\hat{u}_{y\mathbf{k}}(t))^T$. The *hydrodynamic matrix*, \mathcal{L} , is given by

$$\mathcal{L} = \begin{pmatrix} 0 & 0 & \phi_0 k_x & \phi_0 k_y \\ \bar{\omega}_\phi & \bar{\omega}_\theta - \bar{\kappa}_0 k^2 & \bar{p}_0 k_x - 2\epsilon\bar{\eta}_0 k_y & \bar{p}_0 k_y - 2\epsilon\bar{\eta}_0 k_x \\ \epsilon\bar{\eta}_\phi k_y - \bar{p}_\phi k_x & \epsilon\bar{\eta}_\theta k_y - \bar{p}_\theta k_x & -(\bar{\eta}_0 k^2 + \bar{\xi}_0 k_x^2) & -\bar{\xi}_0 k_x k_y - \epsilon \\ \epsilon\bar{\eta}_\phi k_x - \bar{p}_\phi k_y & \epsilon\bar{\eta}_\theta k_x - \bar{p}_\theta k_y & -\bar{\xi}_0 k_x k_y & -(\bar{\eta}_0 k^2 + \bar{\xi}_0 k_y^2) \end{pmatrix} \quad (\text{B19})$$

with a scaled quantity, $\bar{\omega}_\alpha \equiv \omega_\alpha/\phi_0$ ($\alpha = \phi, \theta$). Because the linear operator on the right-hand side of Eq. (B18), i.e., $\mathcal{L} + \epsilon k_x \partial/\partial k_y$, is time-independent, we can separate the time dependence of hydrodynamic modes as $\hat{\phi}_{\mathbf{k}}(t) = f(t)\hat{\psi}(\mathbf{k})$, where Eq. (B18) is rewritten as

$$\frac{1}{f(t)} \frac{\partial f(t)}{\partial t} = \frac{1}{\hat{\psi}(\mathbf{k})} \left(\mathcal{L} + \epsilon k_x \frac{\partial}{\partial k_y}\right)\hat{\psi}(\mathbf{k}) \equiv \lambda \quad (\text{B20})$$

with a constant, λ . Therefore, the time dependence of hydrodynamic modes is found to be $\hat{\phi}_{\mathbf{k}}(t) = f(0)e^{\lambda t}\hat{\psi}(\mathbf{k})$, and the constant λ is given by solving an eigenvalue problem,

$$\left(\mathcal{L} + \epsilon k_x \frac{\partial}{\partial k_y}\right)\hat{\psi}(\mathbf{k}) = \lambda\hat{\psi}(\mathbf{k}), \quad (\text{B21})$$

where λ and $\hat{\psi}(\mathbf{k})$ are redefined as an eigenvalue and right-eigenvector, respectively. For later use, we also introduce a left-eigenvector, $\tilde{\psi}(\mathbf{k})$, as

$$\tilde{\psi}(\mathbf{k})\left(\mathcal{L} + \epsilon k_x \frac{\partial}{\partial k_y}\right) = \lambda\tilde{\psi}(\mathbf{k}). \quad (\text{B22})$$

2. Perturbation theory

We solve the eigenvalue problems, Eqs. (B21) and (B22), by *perturbation theory*, which is well established for the linear stability analysis of simple shear flows of granular gases. Because the anisotropic decay of energy spectra, $E(\mathbf{k})$, is observed in quasistatic flows, $\epsilon \equiv \dot{\gamma}t_m \ll 1$, we use ϵ as a small expansion parameter, where the hydrodynamic matrix, eigenvalue, and eigenvectors are expanded into the power series of ϵ as

$$\mathcal{L} = \mathcal{L}_0 + \epsilon\mathcal{L}_1 + \epsilon^2\mathcal{L}_2, \quad (\text{B23})$$

$$\lambda^{(l)} = \lambda_0^{(l)} + \epsilon\lambda_1^{(l)} + \epsilon^2\lambda_2^{(l)} + \dots, \quad (\text{B24})$$

$$\hat{\psi}^{(l)} = \hat{\psi}_0^{(l)} + \epsilon\hat{\psi}_1^{(l)} + \epsilon^2\hat{\psi}_2^{(l)} + \dots, \quad (\text{B25})$$

$$\tilde{\psi}^{(l)} = \tilde{\psi}_0^{(l)} + \epsilon\tilde{\psi}_1^{(l)} + \epsilon^2\tilde{\psi}_2^{(l)} + \dots, \quad (\text{B26})$$

respectively. In Eqs. (B24)–(B26), the upper script represents each mode ($l = 1, \dots, 4$) and the matrices on the right-hand-side of Eq. (B23) are given by

$$\mathcal{L}_0 = \begin{pmatrix} 0 & 0 & \phi_0 k_x & \phi_0 k_y \\ 0 & -\bar{\kappa}_0 k^2 & \bar{p}_0 k_x & \bar{p}_0 k_y \\ -\bar{p}_\phi k_x & -\bar{p}_\theta k_x & -(\bar{\eta}_0 k^2 + \bar{\xi}_0 k_x^2) & -\bar{\xi}_0 k_x k_y \\ -\bar{p}_\phi k_y & -\bar{p}_\theta k_y & -\bar{\xi}_0 k_x k_y & -(\bar{\eta}_0 k^2 + \bar{\xi}_0 k_y^2) \end{pmatrix}, \quad (\text{B27})$$

$$\mathcal{L}_1 = \begin{pmatrix} 0 & 0 & 0 & 0 \\ 0 & 0 & -2\bar{\eta}_0 k_y & -2\bar{\eta}_0 k_x \\ \bar{\eta}_\phi k_y & \bar{\eta}_\theta k_y & 0 & -1 \\ \bar{\eta}_\phi k_x & \bar{\eta}_\theta k_x & 0 & 0 \end{pmatrix}, \quad (\text{B28})$$

$$\mathcal{L}_2 = \begin{pmatrix} 0 & 0 & 0 & 0 \\ \bar{\Omega}_\phi & \bar{\Omega}_\theta & 0 & 0 \\ 0 & 0 & 0 & 0 \\ 0 & 0 & 0 & 0 \end{pmatrix}, \quad (\text{B29})$$

respectively, where the coefficients associated with the energy balance, Eq. (B9), were scaled as $\bar{\omega}_\alpha \equiv \epsilon^2 \bar{\Omega}_\alpha$ ($\alpha = \phi, \theta$). Then, substituting the power series, Eqs. (B23)–(B26), into the eigenvalue problems, Eqs. (B21) and (B22), we collect each order term of the perturbation parameter, ϵ .

First, we find *zeroth-order equations* as

$$\mathcal{L}_0 \hat{\psi}_0^{(l)} = \lambda_0^{(l)} \hat{\psi}_0^{(l)}, \quad (\text{B30})$$

$$\tilde{\psi}_0^{(l)} \mathcal{L}_0 = \lambda_0^{(l)} \tilde{\psi}_0^{(l)}. \quad (\text{B31})$$

In Appendix C, we solve Eqs. (B30) and (B31) in a long-wavelength limit, $k \rightarrow 0$, where the eigenvalues, right-eigenvectors, and left-eigenvectors are approximated to Eqs. (C32)–(C36), respectively.

Next, we find a *first-order equation* as

$$\lambda_1^{(l)} \hat{\psi}_0^{(l)} = (\mathcal{L}_0 - \lambda_0^{(l)}) \hat{\psi}_1^{(l)} + \left(\mathcal{L}_1 + k_x \frac{\partial}{\partial k_y} \right) \hat{\psi}_0^{(l)}. \quad (\text{B32})$$

Multiplying the left-eigenvector, $\tilde{\psi}_0^{(l)}$, to Eq. (B32), we find a first-order correction to the eigenvalue as

$$\lambda_1^{(l)} = \tilde{\psi}_0^{(l)} \left(\mathcal{L}_1 + k_x \frac{\partial}{\partial k_y} \right) \hat{\psi}_0^{(l)}, \quad (\text{B33})$$

where the orthonormality, $\tilde{\psi}_0^{(i)} \hat{\psi}_0^{(j)} = \delta_{ij}$, was used (see Appendix C) and the first term on the right-hand side of Eq. (B32) was vanished because of $\tilde{\psi}_0^{(l)} (\mathcal{L}_0 - \lambda_0^{(l)}) = 0$ [see Eq. (B31)]. To determine the first-order correction to the right-eigenvector, we write $\hat{\psi}_1^{(l)}$ as a linear combination of $\hat{\psi}_0^{(j)}$, i.e.,

$$\hat{\psi}_1^{(l)} = \sum_{j=1}^4 a_j^{(l)} \hat{\psi}_0^{(j)}, \quad (\text{B34})$$

where $a_j^{(l)}$ ($j, l = 1, \dots, 4$) is defined as a coefficient of $\hat{\psi}_0^{(j)}$. Then, the first-order equation (B32) is rewritten as

$$\lambda_1^{(l)} \hat{\psi}_0^{(l)} = \sum_{j=1}^4 (\lambda_0^{(j)} - \lambda_0^{(l)}) a_j^{(l)} \hat{\psi}_0^{(j)} + \left(\mathcal{L}_1 + k_x \frac{\partial}{\partial k_y} \right) \hat{\psi}_0^{(l)}, \quad (\text{B35})$$

where we used $\mathcal{L}_0 \hat{\psi}_1^{(l)} = \sum_j a_j^{(l)} \mathcal{L}_0 \hat{\psi}_0^{(j)} = \sum_j a_j^{(l)} \lambda_0^{(j)} \hat{\psi}_0^{(j)}$. Multiplying the left-eigenvector, $\tilde{\psi}_0^{(n)}$ ($n \neq l$), to Eq. (B35), we find the coefficient as

$$a_n^{(l)} = \frac{1}{\lambda_0^{(l)} - \lambda_0^{(n)}} \tilde{\psi}_0^{(n)} \left(\mathcal{L}_1 + k_x \frac{\partial}{\partial k_y} \right) \hat{\psi}_0^{(l)}. \quad (\text{B36})$$

Note that we cannot determine the coefficients for $n = l$ from Eq. (B36) and thus simply assume $a_l^{(l)} = 0$, where we calculate

explicit forms of the coefficients, $a_n^{(l)}$ ($n \neq l$), in Appendix D. From Eqs. (B25), (B34), and (B36), we find that the right-eigenvectors are given by Eqs. (6)–(8) in the first-order approximation of ϵ , where the functions, $f_n^{(l)}$ and $g_n^{(l)}$, in Table I represent the real and imaginary parts of the coefficient, $a_n^{(l)}$, respectively.

APPENDIX C: THE ZERO-ORDER EIGENVALUE PROBLEMS

In this appendix, we solve the zeroth-order eigenvalue problems, Eqs. (B30) and (B31), in a long-wavelength limit, $k \rightarrow 0$ (Appendix C 1), and we examine the *relaxation time* of each hydrodynamic mode (Appendix C 2).

1. Perturbation theory

We expand the zeroth-order hydrodynamic matrix, eigenvalue, and right- and left-eigenvectors into the power series of small wave number, $k \ll 1$, as

$$\mathcal{L}_0 = k \mathcal{M}_1 + k^2 \mathcal{M}_2, \quad (\text{C1})$$

$$\lambda_0^{(l)} = k \mathcal{S}_1^{(l)} + k^2 \mathcal{S}_2^{(l)} + k^3 \mathcal{S}_3^{(l)} + \dots, \quad (\text{C2})$$

$$\hat{\psi}_0^{(l)} = \hat{\xi}_0^{(l)} + k \hat{\xi}_1^{(l)} + k^2 \hat{\xi}_2^{(l)} + \dots, \quad (\text{C3})$$

$$\tilde{\psi}_0^{(l)} = \tilde{\xi}_0^{(l)} + k \tilde{\xi}_1^{(l)} + k^2 \tilde{\xi}_2^{(l)} + \dots, \quad (\text{C4})$$

respectively ($l = 1, \dots, 4$). On the right-hand side of Eq. (C1), the matrices are introduced as

$$\mathcal{M}_1 = \begin{pmatrix} 0 & 0 & \phi_0 \hat{k}_x & \phi_0 \hat{k}_y \\ 0 & 0 & \bar{p}_0 \hat{k}_x & \bar{p}_0 \hat{k}_y \\ -\bar{p}_\phi \hat{k}_x & -\bar{p}_\theta \hat{k}_x & 0 & 0 \\ -\bar{p}_\phi \hat{k}_y & -\bar{p}_\theta \hat{k}_y & 0 & 0 \end{pmatrix}, \quad (\text{C5})$$

$$\mathcal{M}_2 = \begin{pmatrix} 0 & 0 & 0 & 0 \\ 0 & -\bar{\kappa}_0 & 0 & 0 \\ 0 & 0 & -(\bar{\eta}_0 + \bar{\xi}_0 \hat{k}_x^2) & -\bar{\xi}_0 \hat{k}_x \hat{k}_y \\ 0 & 0 & -\bar{\xi}_0 \hat{k}_x \hat{k}_y & -(\bar{\eta}_0 + \bar{\xi}_0 \hat{k}_y^2) \end{pmatrix}, \quad (\text{C6})$$

respectively, where $\hat{k}_\alpha \equiv k_\alpha / k$ ($\alpha = x, y$) represents each component of the normalized wave number vector. Substituting the power series, Eqs. (C1)–(C4), into the zeroth-order eigenvalue problems, Eqs. (B30) and (B31), and collecting each order term of the wave number, k , we find the first

nontrivial equations as

$$\mathcal{M}_1 \hat{\xi}_0^{(l)} = \varsigma_1^{(l)} \hat{\xi}_0^{(l)}, \quad (\text{C7})$$

$$\tilde{\xi}_0^{(l)} \mathcal{M}_1 = \varsigma_1^{(l)} \tilde{\xi}_0^{(l)}. \quad (\text{C8})$$

The eigenvalues, $\varsigma_1^{(l)}$, are readily found to be

$$\varsigma_1^{(1)} = \varsigma_1^{(2)} = 0, \quad \varsigma_1^{(3)} = -\varsigma_1^{(4)} = I \frac{J}{\phi_0} \quad (\text{C9})$$

with a constant, $J \equiv \sqrt{p_0 p_\theta + \phi_0^2 p_\phi}$, where corresponding right- and left-eigenvectors are given by

$$\hat{\xi}_0^{(1)} = \left(\frac{p_\theta}{J}, -\frac{p_\phi}{J}, 0, 0 \right)^T, \quad (\text{C10})$$

$$\hat{\xi}_0^{(2)} = (0, 0, \hat{k}_y, -\hat{k}_x)^T, \quad (\text{C11})$$

$$\hat{\xi}_0^{(3)} = \left(\frac{\phi_0^2}{\sqrt{2}J}, \frac{p_0}{\sqrt{2}J}, I \frac{\hat{k}_x}{\sqrt{2}}, I \frac{\hat{k}_y}{\sqrt{2}} \right)^T, \quad (\text{C12})$$

$$\hat{\xi}_0^{(4)} = \left(\frac{\phi_0^2}{\sqrt{2}J}, \frac{p_0}{\sqrt{2}J}, -I \frac{\hat{k}_x}{\sqrt{2}}, -I \frac{\hat{k}_y}{\sqrt{2}} \right)^T, \quad (\text{C13})$$

and

$$\tilde{\xi}_0^{(1)} = \left(\frac{p_0}{J}, -\frac{\phi_0^2}{J}, 0, 0 \right), \quad (\text{C14})$$

$$\tilde{\xi}_0^{(2)} = (0, 0, \hat{k}_y, -\hat{k}_x), \quad (\text{C15})$$

$$\tilde{\xi}_0^{(3)} = \left(\frac{p_\phi}{\sqrt{2}J}, \frac{p_\theta}{\sqrt{2}J}, -I \frac{\hat{k}_x}{\sqrt{2}}, -I \frac{\hat{k}_y}{\sqrt{2}} \right), \quad (\text{C16})$$

$$\tilde{\xi}_0^{(4)} = \left(\frac{p_\phi}{\sqrt{2}J}, \frac{p_\theta}{\sqrt{2}J}, I \frac{\hat{k}_x}{\sqrt{2}}, I \frac{\hat{k}_y}{\sqrt{2}} \right), \quad (\text{C17})$$

respectively. It is readily found that the orthonormality, $\tilde{\xi}_0^{(i)} \hat{\xi}_0^{(j)} = \delta_{ij}$, is satisfied.

Because the first two eigenvalues are degenerated to zero, i.e., $\varsigma_1^{(1)} = \varsigma_1^{(2)} = 0$, we reformulate the expansion of right-eigenvectors, Eq. (C3), as

$$\hat{\psi}_0^{(l)} = \hat{\xi}_0^{(l)} + k \hat{\xi}_1^{(l)} + k^2 \hat{\xi}_2^{(l)} + \dots \quad (\text{C18})$$

for the eigenmodes, $l = 1$ and 2 , where the leading-order term was replaced with a linear combination of $\hat{\xi}_0^{(l)}$, i.e.,

$$\hat{\xi}_0^{(l)} \equiv b_1^{(l)} \hat{\xi}_0^{(1)} + b_2^{(l)} \hat{\xi}_0^{(2)} \quad (\text{C19})$$

with coefficients $b_j^{(l)}$ ($l, j = 1, 2$). Then, the next nontrivial equation in the order of $O(k^2)$ is found to be

$$\mathcal{M}_1 \hat{\xi}_1^{(l)} + \mathcal{M}_2 \hat{\xi}_0^{(l)} = \varsigma_1^{(l)} \hat{\xi}_1^{(l)} + \varsigma_2^{(l)} \hat{\xi}_0^{(l)}. \quad (\text{C20})$$

Because of the zero eigenvalues, $\varsigma_1^{(1)} = \varsigma_1^{(2)} = 0$, Eq. (C20) is reduced to

$$\mathcal{M}_1 \hat{\xi}_1^{(l)} + \mathcal{M}_2 \{b_1^{(l)} \hat{\xi}_0^{(1)} + b_2^{(l)} \hat{\xi}_0^{(2)}\} = \varsigma_2^{(l)} \{b_1^{(l)} \hat{\xi}_0^{(1)} + b_2^{(l)} \hat{\xi}_0^{(2)}\}. \quad (\text{C21})$$

Multiplying the left-eigenvector, $\tilde{\xi}_0^{(j)}$ ($j = 1, 2$), to Eq. (C21), we find that

$$\tilde{\xi}_0^{(j)} \mathcal{M}_2 \{b_1^{(l)} \hat{\xi}_0^{(1)} + b_2^{(l)} \hat{\xi}_0^{(2)}\} = \varsigma_2^{(l)} \{b_1^{(l)} \delta_{j1} + b_2^{(l)} \delta_{j2}\}, \quad (\text{C22})$$

where the first term on the left-hand side of Eq. (C21) was vanished as $\tilde{\xi}_0^{(j)} \mathcal{M}_1 = 0$. Note that Eq. (C22) is explicitly written as

$$\begin{pmatrix} \tilde{\xi}_0^{(1)} \mathcal{M}_2 \hat{\xi}_0^{(1)} & \tilde{\xi}_0^{(1)} \mathcal{M}_2 \hat{\xi}_0^{(2)} \\ \tilde{\xi}_0^{(2)} \mathcal{M}_2 \hat{\xi}_0^{(1)} & \tilde{\xi}_0^{(2)} \mathcal{M}_2 \hat{\xi}_0^{(2)} \end{pmatrix} \begin{pmatrix} b_1^{(l)} \\ b_2^{(l)} \end{pmatrix} = \varsigma_2^{(l)} \begin{pmatrix} b_1^{(l)} \\ b_2^{(l)} \end{pmatrix}, \quad (\text{C23})$$

where each element of the matrix, $\tilde{\xi}_0^{(j)} \mathcal{M}_2 \hat{\xi}_0^{(l)}$, is given by

$$\tilde{\xi}_0^{(1)} \mathcal{M}_2 \hat{\xi}_0^{(1)} = -\frac{\phi_0 \kappa_0 p_\phi}{J^2} k^2, \quad (\text{C24})$$

$$\tilde{\xi}_0^{(1)} \mathcal{M}_2 \hat{\xi}_0^{(2)} = 0, \quad (\text{C25})$$

$$\tilde{\xi}_0^{(2)} \mathcal{M}_2 \hat{\xi}_0^{(1)} = 0, \quad (\text{C26})$$

$$\tilde{\xi}_0^{(2)} \mathcal{M}_2 \hat{\xi}_0^{(2)} = -\frac{\eta_0}{\phi_0} k^2, \quad (\text{C27})$$

i.e., the matrix is diagonal. Thus, we readily find that the second-order corrections to the eigenvalues are given by

$$\varsigma_2^{(1)} = -\frac{\phi_0 \kappa_0 p_\phi}{J^2} k^2, \quad \varsigma_2^{(2)} = -\frac{\eta_0}{\phi_0} k^2, \quad (\text{C28})$$

where the coefficients are determined as $(b_1^{(1)}, b_2^{(1)})^T = (1, 0)^T$ and $(b_1^{(2)}, b_2^{(2)})^T = (0, 1)^T$.

Next, we calculate the second-order corrections to the third and fourth eigenvalues. For $l = 3$ and 4 , the equation in the order of $O(k^2)$ is found to be

$$\mathcal{M}_1 \hat{\xi}_1^{(l)} + \mathcal{M}_2 \hat{\xi}_0^{(l)} = \varsigma_1^{(l)} \hat{\xi}_1^{(l)} + \varsigma_2^{(l)} \hat{\xi}_0^{(l)}. \quad (\text{C29})$$

Multiplying the left-eigenvector, $\tilde{\xi}_0^{(l)}$, to Eq. (C29), we find that

$$\varsigma_2^{(l)} = \tilde{\xi}_0^{(l)} \mathcal{M}_2 \hat{\xi}_0^{(l)}, \quad (\text{C30})$$

where we used $\tilde{\xi}_0^{(l)} \mathcal{M}_1 \hat{\xi}_1^{(l)} = \varsigma_1^{(l)} \tilde{\xi}_0^{(l)} \hat{\xi}_1^{(l)}$. Then, it is readily found that the second-order corrections to the third and fourth eigenvalues are given by

$$\varsigma_2^{(3)} = \varsigma_2^{(4)} = -\frac{1}{2\phi_0} \left(\eta_0 + \xi_0 + \frac{\kappa_0 p_0 p_\theta}{J^2} \right). \quad (\text{C31})$$

In summary, the eigenvalues of the zeroth-order hydrodynamic matrix, \mathcal{L}_0 , are given by

$$\lambda_0^{(1)} = -\frac{\phi_0 \kappa_0 p_\phi}{J^2} k^2, \quad (\text{C32})$$

$$\lambda_0^{(2)} = -\frac{\eta_0}{\phi_0} k^2, \quad (\text{C33})$$

$$\lambda_0^{(3)} = -\frac{1}{2\phi_0} \left(\eta_0 + \xi_0 + \frac{\kappa_0 p_0 p_\theta}{J^2} \right) k^2 + I \frac{J}{\phi_0} k, \quad (\text{C34})$$

$$\lambda_0^{(4)} = -\frac{1}{2\phi_0} \left(\eta_0 + \xi_0 + \frac{\kappa_0 p_0 p_\theta}{J^2} \right) k^2 - I \frac{J}{\phi_0} k, \quad (\text{C35})$$

in the order of $O(k^2)$, where the right- and left-eigenvectors are given by

$$\hat{\psi}_0^{(l)} = \hat{\xi}_0^{(l)}, \quad \tilde{\psi}_0^{(l)} = \tilde{\xi}_0^{(l)}, \quad (\text{C36})$$

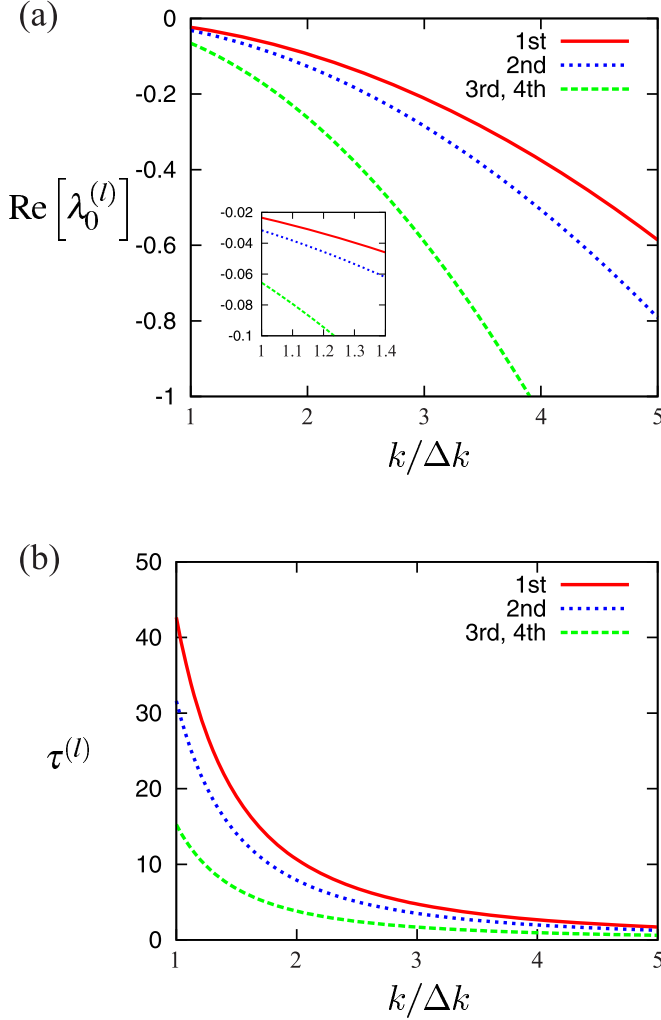


FIG. 6. (a) Real parts of the eigenvalues in the leading order of ϵ , i.e., $\text{Re}[\lambda_0^{(l)}]$ ($l = 1, \dots, 4$), where the inset shows a zoom-in to small wave numbers. Real parts of the third and fourth eigenvalues are equivalent, i.e., $\text{Re}[\lambda_0^{(3)}] = \text{Re}[\lambda_0^{(4)}]$. (b) Relaxation time of each hydrodynamic mode estimated as $\tau^{(l)} \simeq -1/\text{Re}[\lambda_0^{(l)}]$. In both (a) and (b), the red solid, blue dotted, and green broken lines correspond to the modes, $l = 1, 2$, and 3 (or 4), respectively, and $\Delta k \equiv 2\pi/L$ with the linear system size, L , is the increment of wave number.

respectively ($l = 1, \dots, 4$), in the leading order of k . Note that the eigenvectors, Eq. (C36), satisfy the orthonormality, i.e., $\tilde{\psi}_0^{(i)} \hat{\psi}_0^{(j)} = \delta_{ij}$.

2. Relaxation time

The relaxation time of each hydrodynamic mode is given by the inverse of the real part of the eigenvalue as $\tau^{(l)} \equiv -1/\text{Re}[\lambda^{(l)}]$ ($l = 1, \dots, 4$). Since the eigenvalues have been calculated as Eqs. (C32)–(C35) in the leading order of ϵ , we approximate the relaxation time as $\tau^{(l)} \simeq -1/\text{Re}[\lambda_0^{(l)}]$ to examine its magnitude. Figure 6(a) displays the real part of each eigenvalue, $\text{Re}[\lambda_0^{(l)}]$, where all the real parts are negative and decreasing functions of the wave number, i.e., $\text{Re}[\lambda_0^{(l)}] \propto -k^2$. In this figure, the area fraction is given by $\phi_0 = 0.84$ and the first mode is always the largest one so that

the relaxation time of the first mode is always the longest one [Fig. 6(b)].

APPENDIX D: EXPLICIT CALCULATIONS OF THE COEFFICIENTS FOR THE FIRST-ORDER CORRECTION TO RIGHT-EIGENVECTORS

In this Appendix, we explicitly calculate the coefficients, $a_n^{(l)}$ [Eq. (B36)], for the first-order corrections to right-eigenvectors, $\hat{\psi}_1^{(l)}$ [Eq. (B34)], where $n, l = 1, \dots, 4$.

First, we introduce a diagonal matrix as

$$\Lambda \equiv \begin{pmatrix} \lambda^{(1)} & 0 & 0 & 0 \\ 0 & \lambda^{(2)} & 0 & 0 \\ 0 & 0 & \lambda^{(3)} & 0 \\ 0 & 0 & 0 & \lambda^{(4)} \end{pmatrix}, \quad (\text{D1})$$

where each diagonal element corresponds to each eigenvalue of the hydrodynamic matrix, \mathcal{L} . Then, the power series of the eigenvalue, Eq. (B24), can be written in matrix form as

$$\Lambda = \Lambda_0 + \epsilon \Lambda_1 + \epsilon^2 \Lambda_2 + \dots, \quad (\text{D2})$$

where each diagonal matrix on the right-hand side, Λ_n ($n = 0, 1, 2, \dots$), is given by

$$\Lambda_n \equiv \begin{pmatrix} \lambda_n^{(1)} & 0 & 0 & 0 \\ 0 & \lambda_n^{(2)} & 0 & 0 \\ 0 & 0 & \lambda_n^{(3)} & 0 \\ 0 & 0 & 0 & \lambda_n^{(4)} \end{pmatrix}. \quad (\text{D3})$$

If we write the zeroth-order right-eigenvectors, $\hat{\psi}_0^{(l)}$ [Eq. (C36)], in matrix form as

$$\Psi_0 \equiv (\hat{\psi}_0^{(1)}, \hat{\psi}_0^{(2)}, \hat{\psi}_0^{(3)}, \hat{\psi}_0^{(4)}) = \begin{pmatrix} \frac{p_0}{J} & 0 & \frac{\phi_0^2}{\sqrt{2}J} & \frac{\phi_0^2}{\sqrt{2}J} \\ -\frac{p_0}{J} & 0 & \frac{p_0}{\sqrt{2}J} & \frac{p_0}{\sqrt{2}J} \\ 0 & \hat{k}_y & \frac{I\hat{k}_x}{\sqrt{2}} & -\frac{I\hat{k}_x}{\sqrt{2}} \\ 0 & -\hat{k}_x & \frac{I\hat{k}_y}{\sqrt{2}} & -\frac{I\hat{k}_y}{\sqrt{2}} \end{pmatrix}, \quad (\text{D4})$$

TABLE II. Explicit forms of the coefficients, $a_n^{(l)}$, for $n \neq l$, where only $a_1^{(2)}$ and $a_2^{(1)}$ are real numbers and the other elements are given by complex conjugates as $a_1^{(4)} = a_1^{(3)*}$, $a_2^{(4)} = a_2^{(3)*}$, $a_4^{(1)} = a_3^{(1)*}$, $a_4^{(2)} = a_3^{(2)*}$, and $a_4^{(3)} = a_3^{(4)*}$ (* indicates the complex conjugate). Here, $J \equiv \sqrt{p_0 p_\theta + \phi_0^2 p_\phi}$ and $A \equiv (\eta_0 + \xi_0 + \kappa_0 p_0 p_\theta / J^2) / 2\phi_0$.

$$\begin{aligned} a_1^{(2)} &= -\frac{2\phi_0^2 \eta_0 J}{\eta_0 J^2 - \phi_0^2 \kappa_0 p_\phi} \frac{k_x^2 - k_y^2}{k^3} \\ a_1^{(3)} &= \frac{2\sqrt{2}\phi_0^2 \eta_0 J (J^3 + I\phi_0(\phi_0 \kappa_0 p_\phi - AJ^2)k)}{\phi_0^2 (\phi_0 \kappa_0 p_\phi - AJ^2)^2 k^2 + J^6} \frac{k_x k_y}{k^2} \\ a_2^{(1)} &= \frac{J(p_\theta \eta_\phi - p_\phi \eta_\theta)}{\eta_0 J^2 - \phi_0^2 \kappa_0 p_\phi} \frac{k_y^2 - k_x^2}{k^3} \\ a_2^{(3)} &= \frac{\sqrt{2}b\phi_0(\eta_0 - \phi_0 A)(k_x^2 - k_y^2) - J}{\sqrt{2}((\eta_0 - \phi_0 A)^2 k^2 + J^2)k} + \frac{I(\sqrt{2}bJ(k_x^2 - k_y^2) - \phi_0(\eta_0 - \phi_0 A)k^2)}{\sqrt{2}((\eta_0 - \phi_0 A)^2 k^2 + J^2)k^2} \\ a_3^{(1)} &= \frac{\sqrt{2}J(p_\theta \eta_\phi - p_\phi \eta_\theta)(J^3 + I\phi_0(\phi_0 \kappa_0 p_\phi - AJ^2)k)}{\phi_0^2 (\phi_0 \kappa_0 p_\phi - AJ^2)^2 k^2 + J^6} \frac{k_x k_y}{k^2} \\ a_3^{(2)} &= \frac{\sqrt{2}\phi_0 J^2 k_x^2 - p_\theta \eta_0 (\eta_0 - \phi_0 A)(k_x^2 - k_y^2)}{J((\eta_0 - \phi_0 A)^2 k^2 + J^2)k^3} \\ &\quad + \frac{\sqrt{2}I(p_\theta \eta_0 (k_x^2 - k_y^2) + \phi_0(\eta_0 - \phi_0 A)k_x^2)}{((\eta_0 - \phi_0 A)^2 k^2 + J^2)k^2} \\ a_3^{(4)} &= \frac{\phi_0 c_m}{2J} \frac{k_x k_y}{k^2} + I \frac{\phi_0}{4J} \frac{k_x k_y}{k^3} \end{aligned}$$

the zeroth-order equation (B30) is rewritten as

$$\mathcal{L}_0 \Psi_0 = \Psi_0 \Lambda_0. \quad (\text{D5})$$

We also introduce a matrix form of the zeroth-order left-eigenvectors, $\tilde{\psi}_0^{(l)}$ [Eq. (C36)], as

$$\Psi_0^{-1} \equiv \begin{pmatrix} \tilde{\psi}_0^{(1)} \\ \tilde{\psi}_0^{(2)} \\ \tilde{\psi}_0^{(3)} \\ \tilde{\psi}_0^{(4)} \end{pmatrix} = \begin{pmatrix} \frac{p_0}{J} & -\frac{\phi_0^2}{J} & 0 & 0 \\ 0 & 0 & \hat{k}_y & -\hat{k}_x \\ \frac{p_\theta}{\sqrt{2}J} & \frac{p_\theta}{\sqrt{2}J} & -\frac{I\hat{k}_x}{\sqrt{2}} & -\frac{I\hat{k}_y}{\sqrt{2}} \\ \frac{p_\theta}{\sqrt{2}J} & \frac{p_\theta}{\sqrt{2}J} & \frac{I\hat{k}_x}{\sqrt{2}} & \frac{I\hat{k}_y}{\sqrt{2}} \end{pmatrix} \quad (\text{D6})$$

such that Ψ_0 and Ψ_0^{-1} are orthonormal, i.e., $\Psi_0^{-1} \Psi_0 = \mathcal{I}$ with the identity matrix, \mathcal{I} . Then, we find that a part of the right-hand-side of Eq. (B36), i.e., $\tilde{\psi}_0^{(n)} (\mathcal{L}_1 + k_x \partial / \partial k_y) \hat{\psi}_0^{(l)}$, is given by the (n, l) element of the matrix,

$$\Pi \equiv \Psi_0^{-1} \left(\mathcal{L}_1 + k_x \frac{\partial}{\partial k_y} \right) \Psi_0. \quad (\text{D7})$$

By using Eqs. (B28), (D4), and (D6), and the derivatives of wave numbers, $k_x \partial \hat{k}_x / \partial k_y = -\hat{k}_x^2 \hat{k}_y$ and $k_x \partial \hat{k}_y / \partial k_y = \hat{k}_x^3$, we calculate each element of the matrix, Π , as

$$\Pi = \begin{pmatrix} 0 & \frac{2\phi_0^2 \bar{\eta}_0}{J} \frac{k_y^2 - k_x^2}{k} & I \frac{2\sqrt{2}\phi_0^2 \bar{\eta}_0}{J} \frac{k_x k_y}{k} & -I \frac{2\sqrt{2}\phi_0^2 \bar{\eta}_0}{J} \frac{k_x k_y}{k} \\ a \frac{k_y^2 - k_x^2}{k} & \frac{k_x k_y}{k^2} & b \frac{k_y^2 - k_x^2}{k} - \frac{I}{\sqrt{2}} & b \frac{k_y^2 - k_x^2}{k} + \frac{I}{\sqrt{2}} \\ -\sqrt{2} I a \frac{k_x k_y}{k} & \frac{\sqrt{2} p_\theta \bar{\eta}_0}{J} \frac{k_x^2 - k_y^2}{k} - \sqrt{2} I \hat{k}_x^2 & -\frac{k_x k_y}{2k^2} - I c_p \frac{k_x k_y}{k} & \frac{k_x k_y}{2k^2} - I c_m \frac{k_x k_y}{k} \\ \sqrt{2} I a \frac{k_x k_y}{k} & \frac{\sqrt{2} p_\theta \bar{\eta}_0}{J} \frac{k_x^2 - k_y^2}{k} + \sqrt{2} I \hat{k}_x^2 & \frac{k_x k_y}{2k^2} + I c_m \frac{k_x k_y}{k} & -\frac{k_x k_y}{2k^2} + I c_p \frac{k_x k_y}{k} \end{pmatrix}, \quad (\text{D8})$$

where the constants a , b , c_p , and c_m have been introduced as

$$a \equiv \frac{p_\theta \bar{\eta}_\phi - p_\phi \bar{\eta}_\theta}{J}, \quad (\text{D9})$$

$$b \equiv \frac{\phi_0^2 \bar{\eta}_\phi + p_0 \bar{\eta}_\theta}{\sqrt{2} J}, \quad (\text{D10})$$

$$c_p \equiv \frac{\phi_0^2 \bar{\eta}_\phi + p_0 \bar{\eta}_\theta + 2p_\theta \bar{\eta}_0}{J}, \quad (\text{D11})$$

$$c_m \equiv \frac{\phi_0^2 \bar{\eta}_\phi + p_0 \bar{\eta}_\theta - 2p_\theta \bar{\eta}_0}{J}, \quad (\text{D12})$$

respectively. Note that the diagonal elements of Π correspond to the first-order corrections to eigenvalues, Eq. (B33), and its off-diagonal elements correspond to the coefficients for the first-order corrections to right-eigenvectors, Eq. (B36), except for the factor $1/(\lambda_0^{(l)} - \lambda_0^{(n)})$, i.e., $\pi_{ll} = \lambda_1^{(l)}$ and $\pi_{nl} = (\lambda_0^{(l)} - \lambda_0^{(n)}) a_n^{(l)}$ ($n \neq l$) if we write the (n, l) element of Π as π_{nl} . In Table II, we list explicit forms of the coefficients, $a_n^{(l)}$.

-
- [1] J. Lemaitre and J.-L. Chaboche, *Mechanics of Solid Materials* (Cambridge University Press, Cambridge, UK, 1990).
- [2] E. Woldhuis, V. Chikkadi, M. S. van Deen, P. Schall, and M. van Hecke, *Soft Matter* **11**, 7024 (2015).
- [3] K. Saitoh and H. Mizuno, *Soft Matter* **12**, 1360 (2016).
- [4] K. Saitoh and H. Mizuno, *Phys. Rev. E* **94**, 022908 (2016).
- [5] J. T. Jenkins and M. W. Richman, *Phys. Fluids* **28**, 3485 (1985).
- [6] T. Hatano, *J. Phys. Soc. Jpn.* **77**, 123002 (2008).
- [7] M. Otsuki and H. Hayakawa, *Phys. Rev. E* **80**, 011308 (2009).
- [8] O. Poulliquen, *Phys. Rev. Lett.* **93**, 248001 (2004).
- [9] F. Radjai and S. Roux, *Phys. Rev. Lett.* **89**, 064302 (2002).
- [10] B. P. Tighe, E. Woldhuis, J. J. C. Remmers, W. van Saarloos, and M. van Hecke, *Phys. Rev. Lett.* **105**, 088303 (2010).
- [11] C. Heussinger and J.-L. Barrat, *Phys. Rev. Lett.* **102**, 218303 (2009).
- [12] G. Combe, V. Richefeu, M. Stasiak, and A. P. F. Atman, *Phys. Rev. Lett.* **115**, 238301 (2015).
- [13] M. Isobe, *Phys. Rev. E* **68**, 040301(R) (2003).
- [14] A. Furukawa, K. Kim, S. Saito, and H. Tanaka, *Phys. Rev. Lett.* **102**, 016001 (2009).
- [15] S. Mandal, V. Chikkadi, B. Nienhuis, D. Raabe, P. Schall, and F. Varnik, *Phys. Rev. E* **88**, 022129 (2013).
- [16] V. Chikkadi, G. Wegdam, D. Bonn, B. Nienhuis, and P. Schall, *Phys. Rev. Lett.* **107**, 198303 (2011).
- [17] V. Chikkadi, S. Mandal, B. Nienhuis, D. Raabe, F. Varnik, and P. Schall, *Europhys. Lett.* **100**, 56001 (2012).

- [18] C. E. Maloney and M. O. Robbins, *Phys. Rev. Lett.* **102**, 225502 (2009).
- [19] A. Nicolas, J. Rottler, and J.-L. Barrat, *Europhys. J. E* **37**, 50 (2014).
- [20] J. Chattoraj and A. Lemaître, *Phys. Rev. Lett.* **111**, 066001 (2013).
- [21] S. Luding, *J. Phys.: Condens. Matter* **17**, S2623 (2005).
- [22] We have confirmed that our numerical results were quite insensitive to the friction coefficient, μ_m ; see Ref. [3].
- [23] A. W. Lees and S. F. Edwards, *J. Phys. C* **5**, 1921 (1972).
- [24] The system is in a steady state if the applied strain exceeds unity, $\gamma > 1$. During steady states, the ratio of particle stiffness, k_n , to the confining pressure, p , is in the range between $50 < k_n/p < 10^4$.
- [25] If we introduce an arbitrary dynamical variable and its conjugate as $A(\mathbf{r}, t)$ and $A^*(\mathbf{r}', t')$ (which are defined at different positions, $\mathbf{r} \neq \mathbf{r}'$, and time, $t > t'$), respectively, their *spatiotemporal correlation function* is written as $\langle A(\mathbf{r}, t)A^*(\mathbf{r}', t') \rangle = \langle A(\mathbf{r} - \mathbf{r}', t - t')A^*(\mathbf{0}, 0) \rangle$, where the system is assumed to be homogeneous and stationary (or in a steady state) [31]. However, if the system is deformed by simple shear, the relative position, $\mathbf{r} - \mathbf{r}'$, should be replaced with $\mathbf{r} - \mathbf{r}' - \dot{\gamma}(t - t')y\mathbf{e}_x$ such that the correlation function is given by $\langle A(\mathbf{r}, t)A^*(\mathbf{r}', t') \rangle = \langle A(\mathbf{r} - \mathbf{r}' - \dot{\gamma}\tau y\mathbf{e}_x, \tau)A^*(\mathbf{0}, 0) \rangle$ with the duration, $\tau \equiv t - t' > 0$, and its Fourier transform satisfies $\langle A_{\mathbf{k}}(t)A_{\mathbf{k}'}^*(t') \rangle = \langle A_{\mathbf{k}(\tau)}(\tau)A_{-\mathbf{k}}(0) \rangle$, where $A_{\mathbf{k}}(t)$ is the Fourier coefficient of $A(\mathbf{r}, t)$ and $\mathbf{k}(\tau) \equiv (k_x, k_y - \dot{\gamma}\tau k_x)$ is the time-dependent wave number vector. For example, if we replace the dynamical variable with the density fluctuation, $\delta\rho(\mathbf{r}, t)$, the Fourier transform gives the (*self*-)intermediate scattering function as $\langle \delta\rho_{\mathbf{k}(\tau)}(\tau)\delta\rho_{-\mathbf{k}}(0) \rangle$ which has been well studied, e.g. by the mode-coupling theory under simple shear deformations [27]. However, as long as we consider equal-time correlations, $\tau = 0$, the Fourier transforms are time-independent, e.g. the *static structure factor* under shear [27,28]. We also note that correlations and spectra of *non-affine displacements*, $\Delta\mathbf{r}_i(\tau) \equiv \mathbf{r}_i(t) - \mathbf{r}_i(t')$, or related quantities, e.g. *non-affine strain fields*, do depend on time because of their own dependence on the duration, τ [14,19,20].
- [26] A. Onuki, *Phase Transition Dynamics* (Cambridge University Press, Cambridge, UK, 2002).
- [27] K. Miyazaki, D. R. Reichman, and R. Yamamoto, *Phys. Rev. E* **70**, 011501 (2004).
- [28] M. Zhang and G. Szamel, *Phys. Rev. E* **83**, 061407 (2011).
- [29] S. B. Savage, *J. Fluid Mech.* **377**, 1 (1998).
- [30] S. Luding, *Phys. Rev. E* **63**, 042201 (2001).
- [31] J. P. Hansen and I. R. McDonald, *Theory of Simple Liquids*, 3rd ed. (Academic, Elsevier, London, UK, 2006).
- [32] K. Saitoh, S. Takada, and H. Hayakawa, *Soft Matter* **11**, 6371 (2015).
- [33] N. Upadhyaya, L. R. Gómez, and V. Vitelli, *Phys. Rev. X* **4**, 011045 (2014).
- [34] D. V. Denisov, K. A. Lörincz, J. T. Uhl, K. A. Dahmen, and P. Schall, *Nat. Commun.* **7**, 10641 (2015).
- [35] K. Saitoh and H. Hayakawa, *Phys. Rev. E* **75**, 021302 (2007).
- [36] K. Saitoh and H. Hayakawa, *Granular Matter* **13**, 697 (2011).
- [37] K. Saitoh and H. Hayakawa, *Phys. Fluids* **25**, 070606 (2013).